Effects of Deep n-Implants on the Electrons' Transport in Silicon Drift Detectors

Andrea Castoldi, *Member, IEEE*, Chiara Guazzoni, *Member, IEEE*, and Lothar Strüder

***Abstract*—A silicon drift detector has been designed to experimentally verify the effects of deep n-implants on the electrons' transport. Regions of deep n-implants have been introduced underneath the p^+ field strips in close proximity to one detector surface. The presence of deep n-implants reduces the amplitude of the potential perturbation that propagates into the semiconductor volume caused by the segmentation of the p^+ strips. As a consequence higher carrier velocities and more insensitivity to surface properties can be obtained with respect to the conventional design (without deep n-implants). This effect is of particular interest when carrier transport must take place at few micrometers from the surface and when position sensing requires the measurement of the drift time.**

The experimental characterization of the electron velocity as a function of the drift field and the interpretation of the results are reported. At 11 μm from the surface and with a drift field as low as 25 V/cm in presence of deep n-implants we measured an electron velocity of 0.027 cm/μs.

***Index Terms*—Electrons' transport, multilinear silicon drift detectors, position sensing.**

I. Introduction

SINCE the invention of Silicon Drift Detectors in 1983 by E. Gatti and P. Rehak [1] significant improvements have been made in the detector production and new topologies have been introduced. The use of wafers with high quality epitaxial layers in the production of silicon drift detectors assures the full compatibility with the well-established technological production process of fully depleted pn-CCDs [2]. Deep implants of boron and phosphorous at different doses and energy are available. The noise performances achievable with the on-chip input JFET benefit of the high quality of the epitaxial layer allowing to achieve optimum performances in the spectroscopic analysis of the detected photons.

In order to improve rate performances, multilinear silicon drift detectors have been proposed [3], [4] in which the lateral broadening of the signal charge is reduced. In these detectors charge confinement is achieved by displacing the potential minimum for the electrons close to one of the two surfaces of the detector where deep p-implants (*channel-stop* implants) are located inside a high quality epitaxial layer. However, as the electrons are forced to drift closer to one of the detector's surface the sensitivity to the surface properties [5] increases. As a consequence the average drift velocity reduces with respect to the bulk value (bulk electron mobility $\times$ applied drift field) and if we go in close proximity to the surface the potential perturbation introduced by the strip segmentation at a given drift field can be so high to block the electrons drift.

Our research aimed to overcome such degradation of the electron transport by introducing regions of deep n-implants in the middle of the drift channels defined by the channel-stop implants. The deep n-implants cover only the central part of the drift channels and do not overlap with the channel-stop implants. The ionized donors of the deep n-implants favor the confinement of the signal electrons to the center of the drift channel and reduce significantly the potential perturbations along the drift. In this paper, we show a detailed experimental study of the effects of the deep n-implants on the electron transport and on the average electron velocity in silicon drift detectors when the electrons are forced to drift at few micrometers from the detector's surface. Section II gives a detailed description of the detector architecture designed to improve the electron transport. In Section III the results of the experimental characterization are shown. Section IV is devoted to the discussion of the experimental results.

II. "Electron Transport Improvement" Technique

A. Detector Concept

The basic idea to overcome the degradation of the electron transport in a silicon drift detector when the electrons must drift close to one detector side, is to reduce the residual ripple caused by the segmentation of the p^+ field strips in the bottom of the channel. In order to achieve this result we have introduced regions of deep n-implants (Phosphorous, 520 keV, 4×10^{11} cm^{-2}, projected range 0.65 μm) underneath the p^+ field strips in close proximity to one surface of a multilinear silicon drift detector. The detector cross section along the electrons drift path is shown in Fig. 1. As it can be noticed the deep n-implants are interrupted in correspondence of oxide gaps between two contiguous p^+ strips. This is the first time in which arrays of deep n-implants (already used as *channel guide* for charge confinement in fully depleted pn-CCDs [2]) are implanted in Silicon Drift Detectors.

Fig. 2 shows the doping profile along the detector thickness in the first few micrometers from the implanted surface.

Manuscript received November 24, 2001; revised March, 11, 2002. This work was supported by INFN, Istituto Nazionale di Fisica Nucleare–Sezione di Milano.

A. Castoldi is with the Dipartimento di Ingegneria Nucleare Ce.S.N.E.F., Politecnico di Milano, 20133 Milano, Italy, and also with INFN, Sezione di Milano (e-mail: Andrea.Castoldi@polimi.it).

C. Guazzoni is with the Dipartimento di Elettronica e Informazione, Politecnico di Milano, 20133 Milano, Italy, and also with INFN, Sezione di Milano (e-mail: Chiara.Guazzoni@mi.infn.it).

L. Strüder is with the Halbleiterlabor of the Max Planck Institut, D-81279 Munich, Germany (e-mail: lts@hll.mpg.de).

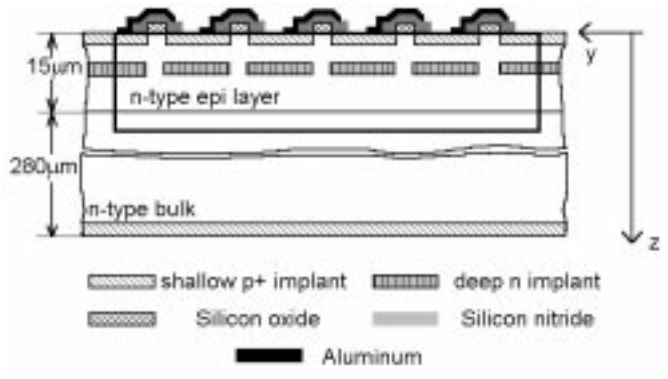

Fig. 1. Scheme of principle of the detector cross section along the electrons' drift direction at the center of a drift channel. The silicon oxide is 220 nm thick and the Silicon nitride is 230 nm thick. The simulation domain is within the bold rectangle.

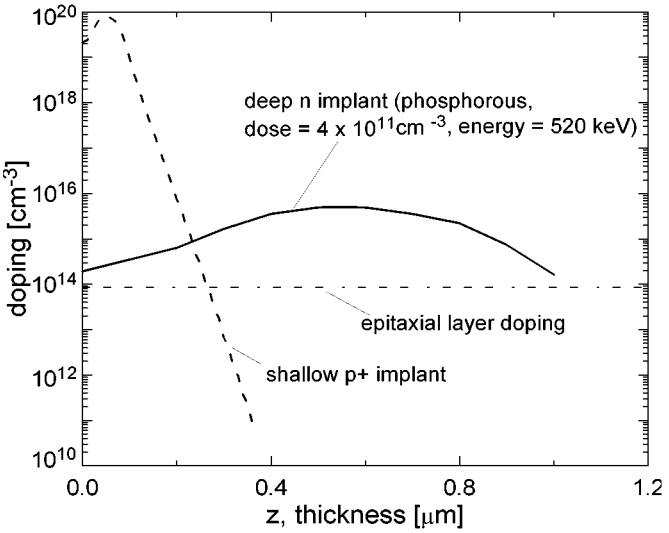

Fig. 2. Doping profile along the detector thickness at the center of a drift channel. The shallow p^+ implant is the one used for the field strips.

B. Simulations

We have simulated both the designed structure with deep n-implanted regions and the conventional structure without deep implants and compared the result of the two simulations. The simulated structure is shown in Fig. 1 for the case of deep n-implant along the drift direction. The applied drift field is 300 V/cm. The charge density at the $Si–SiO_2$ interface has been assumed equal to 2×10^{11} cm^{-2} that is a typical value for this technology. The field plate over the oxide (and nitride) is connected to the strip at lowest negative potential.

In Fig. 3 the potential profile along the drift coordinate at different depths from the front surface is shown both in the conventional case in which no deep implantation is present along the drift channel and in the case of deep n-implants along the drift channel. The presence of deep n-implants tends to lower locally the negative potential which results in a reduction of the peak-to-peak perturbation caused by the segmentation of the p^+ field strips in the bottom of the channel. In this way average drift velocities closer to the bulk value can be obtained at a given drift field and proper work even at very low drift fields is possible with respect to the conventional case (no deep implantation

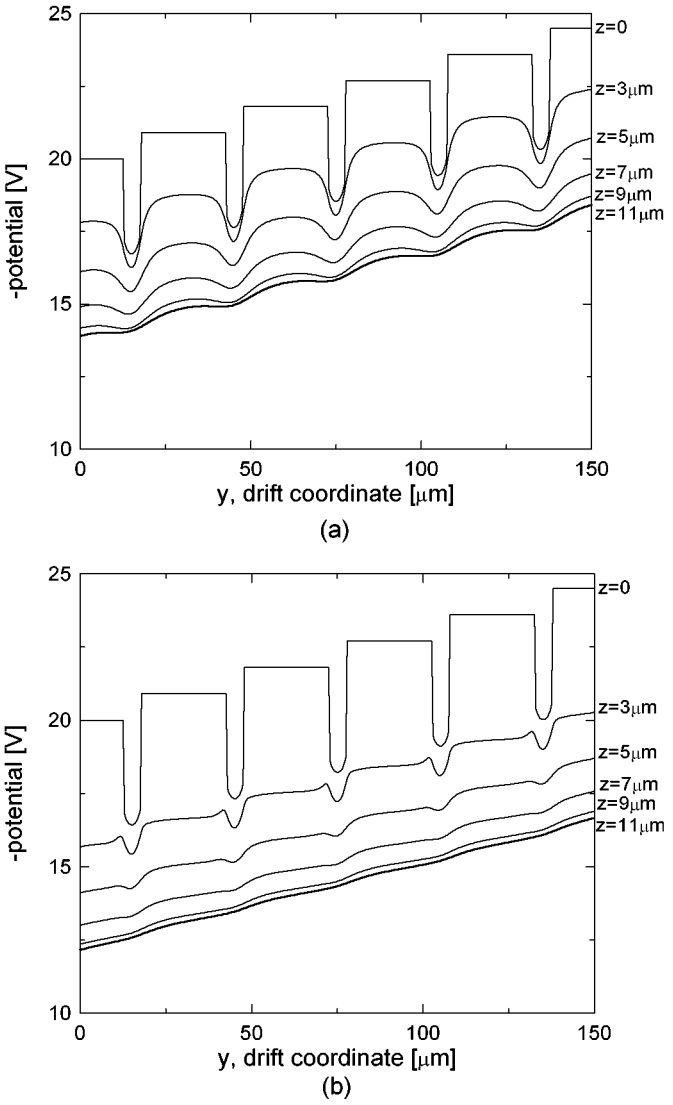

Fig. 3. Two-dimensional simulation of the negative potential close to the front surface along one drift channel. The applied drift field is 300 V/cm. The interface charge density has been assumed equal to 2×10^{11} cm^{-2} that is a typical value for this technology. The field plate over the oxide (and nitride) is connected to the strip at lowest negative potential. The potential profile at the surface ($z = 0$) and at different depths from the front surface up to $z = 11$ μm, where the potential minimum along z is located, is shown in (a) the case of absence of deep n-implants and in (b) the case of presence of deep n-implants.

is present). Moreover, higher stability in the electron transport is achieved as the drift velocity is less sensitive to the properties of the surface. These effects are of interest in drift detectors where the signal electrons drift at few micrometers from the surface (e.g., multilinear silicon drift detectors) and when the electron drift time is required to determine the position of incidence along the drift coordinate.

III. Experimental Characterization

In order to test the effectiveness of such design, an infrared pulsed laser ($\lambda = 904$ nm) has been focused on the front side of the detector in the middle of one drift channel to generate the signal charge and displaced by 30 μm steps (equal to the pitch of the field strips) along the drift direction. The signal

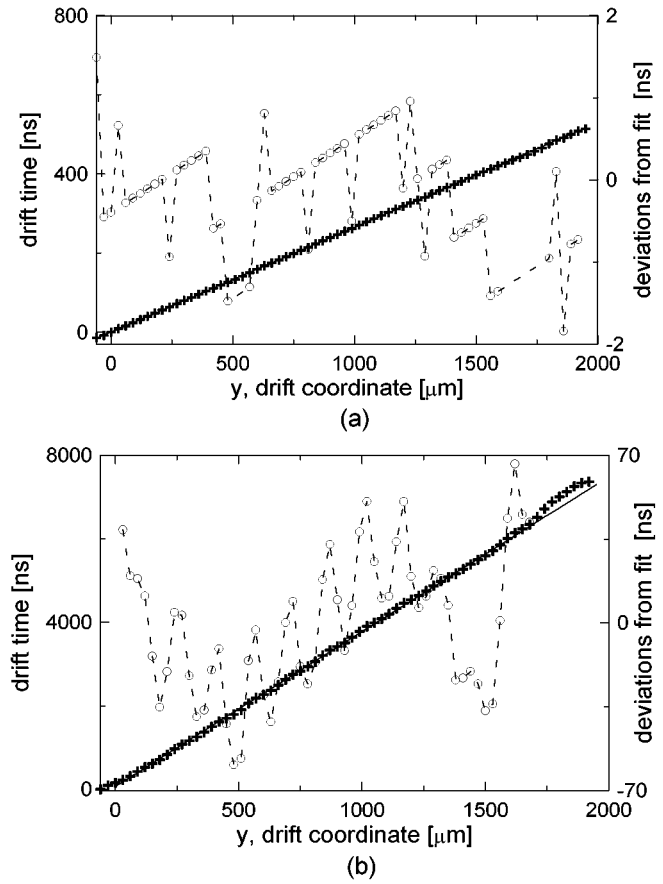

Fig. 4. Drift time measurement at two different drift fields (a) 300 V/cm, (b) 25 V/cm. The nonlinearity at the end of the experimented area are due to side effects in the biasing of the detector. The incident points of the laser spot are spaced by 30 μm (equal to the pitch of the field strips). The circles show the deviations of the experimental points from the linear fit.

pulse induced at the anode is pre-amplified and fed to a bipolar shaper for the optimal detection of the arrival time. The drift time is taken as the interval between the laser trigger and the zero-crossing of the output waveform. The laser intensity was adjusted to generate about 15 000 electrons. Drift fields from values as low as 25 V/cm up to 500 V/cm have been tested. In all these cases the potential minimum is located about 11 μm from the front surface. A shaping time of 250 ns was used for the measurement for drift fields down to 100 V/cm. For lower drift fields a longer shaping time of 3 μs has been used to reduce ballistic deficit. In fact as the drift time increases electron cloud broadening becomes comparable to the shaping time (at 50 V/cm the time broadening of the electron cloud is greater than 200 ns r.m.s.). In Fig. 4(a) the drift time is reported versus the drift coordinate with the detector biased at 300 V/cm. The measured deviations from the linear fit are comparable with the resolution of the acquisition system (1 ns) which is the reason for the observed pattern of Fig. 4(a). In Fig. 4(b) the same measurement is reported with the detector biased at 25 V/cm, the lowest tested drift field. The nonlinearity at the end of the experimented area is due to side effects in the biasing of the detector. For all the tested drift fields the uniformity of the drift velocity is very good.

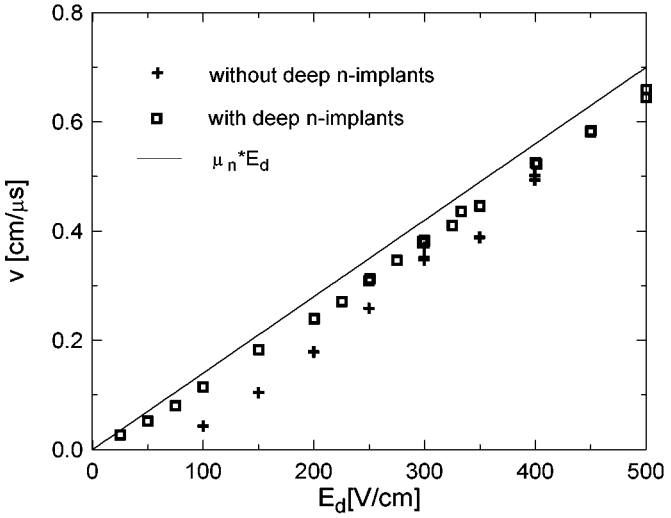

Fig. 5. Average drift velocity as a function of the applied drift field E_d both in presence (empty squares) and in absence (crosses) of deep n-implants. The solid line represents the ideal bulk drift velocity $v_d = \mu_n \times E_d$, where $\mu_n = 1400$ cm^2/(Vs) is the electrons' bulk mobility.

IV. Discussion

Fig. 5 shows the average drift velocity as a function of the applied drift field. It has been derived from the linear fit of the measured drift times versus the drift coordinate. The reduction in the drift field at 11 μm from the front surface with respect to the drift field applied at the front surface due to the uniform back implantation is less than 4% and has been neglected. The solid line represents the ideal bulk velocity $v_d = \mu_n \times E_d$ in a uniform drift field, where we arbitrarily assumed $\mu_n = 1400$ cm^2/(Vs) for the electron bulk mobility. For comparison also the average drift velocities achieved in the same material without deep n-implants are shown.

At 300 V/cm with deep n-implants the average drift velocity is 0.38 cm/μs, showing a reduction of only 9% with respect to the bulk drift velocity to be compared with a velocity reduction of 17% in the conventional case.

The average drift velocity measured at 100 V/cm, the lowest drift field that ensured proper electron transport in the conventional case, is 0.043 cm/μs in the conventional case, showing a reduction of 69% with respect to the nominal drift velocity while with deep n-implants an average drift velocity of 0.11 cm/μs has been measured (18% reduction).

With deep n-implants proper electron drift is possible even at 25 V/cm and the achieved average drift velocity is 0.027 cm/μs, showing a reduction of less than 23% with respect to the nominal drift velocity.

Let us now model the main surface effects that are responsible for the observed non linearity in the electrons' transport.

According to the Laplace equation, a sinusoidal potential perturbation of period P_y

$$\Delta V \sin\left(\frac{2\pi}{P_y}\, y\right) \tag{1}$$

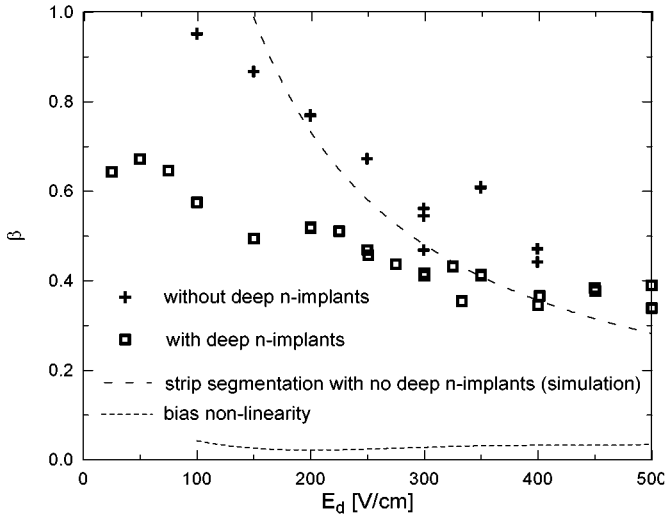

Fig. 6. Values of β (see text) as a function of the applied drift field both in presence (empty squares) and in absence (crosses) of deep n-implants. The values of β calculated from the measured nonlinearity of the bias voltages are also shown with dotted line. The dashed line indicates the values of β simulated by taking into account only the effect of the segmentation of the p+ field strips.

at one surface of the detector with homogeneous Dirichlet conditions at the other surface produces at a depth z a sinusoidal field having approximate amplitude

$$\Delta E \cong \frac{2\pi}{P_y}\,\Delta V \exp\left(-\frac{2\pi}{P_y}\,z\right) \tag{2}$$

that reduces the average electron velocity to [6]

$$v_{av} = \frac{\Delta y}{\int_{y_1}^{y_2} \frac{dy}{v_d(y)}} = (\mu_n \cdot E_d)\sqrt{1-\beta^2} \tag{3}$$

where $\beta = \Delta E/E_d$ is the amplitude of the field perturbation normalized to the drift field.

A first source of nonlinearity is the segmentation of the field strips. It produces a periodic perturbation of the surface potential with a period equal to the strip pitch (=30 μm) and an amplitude depending on the electrostatic properties of the silicon–oxide interface and on the strip geometry. As it can be deduced from the simulations, the perturbation introduced by the segmentation of the field strips can be well described for our purpose as a square wave of period equal to the strip pitch and duty cycle given by the (oxide width/strip pitch) ratio (equal to 1/6 in the present prototype). Expanding this perturbation in Fourier series and retaining only the fundamental term we obtain a good approximation of β at $z = 11$ μm from the front surface.

Another source of nonlinearity is the integrated voltage divider. The nonlinearity of the bias voltages has been measured and can be directly Fourier-analyzed. Also in this case a pure sinusoidal wave well approximates the actual effect at $z = 11$ μm. With these reasonable simplifications we can compute the effect of each source of perturbation on the average velocity separately by means of (3).

In Fig. 6 the values of β are plotted as a function of the drift field, E_d. The experimental points are obtained by solving (3) for β and inserting the measured values of v_{av}. The values of β are shown both in the conventional case in which no deep implantation is present along the drift channel and in the case of deep n-implants along the drift channel. The estimated values of β due to the strip segmentation and bias nonlinearity are also shown. The major contribution to β arises from the segmentation of the field strips while bias nonlinearity has negligible influence on the electron velocity.

As it can be noticed from Fig. 6 in the conventional Silicon Drift Detector β approaches unity (that means no drift is possible) at drift fields of the order of 100 V/cm. By adding the deep n-implants β appears to saturate to 0.65 for drift fields lower than 75 V/cm.

ACKNOWLEDGMENT

The authors would like to thank E. Gatti for many fruitful discussions, P. Holl and the staff of the MPI Halbleiterlabor for the detector production, and S. Masci for the careful bonding of the detector chip.

REFERENCES

[1] E. Gatti and P. Rehak, "Semiconductor Drift Chamber: An application of a novel charge transport scheme," *Nucl. Instrum. Methods*, vol. A225, pp. 608–614, 1984.

[2] L. Strüder, H. Bräuninger, U. Briel, R. Hartmann, G. Hartner, D. Hauff, N. Krause, B. Maier, N. Meidinger, E. Pfeffermann, M. Popp, C. Reppin, R. Richter, D. Stötter, J. Trümper, U. Weber, P. Holl, J. Kemmer, H. Soltau, A. Viehl, and C. v. Zanthier, "A 36 cm^2 large monolithic pn-charge coupled device X-ray detector for the European XMM satellite mission," *Rev. Sci. Instrum.*, vol. 68, pp. 4271–4274, 1997.

[3] A. Castoldi, P. Rehak, and P. Holl, "A new silicon drift detector with reduced lateral diffusion," *Nucl. Instrum. Methods*, vol. A377, pp. 375–380, 1996.

[4] ——, "Signal charge sharing in multilinear silicon drift detectors: Design and experimental characterization," *IEEE Trans. Nucl. Sci.*, vol. 44, pp. 134–141, 1997.

[5] A. Longoni, M. Sampietro, and L. Strüder, "Instability of the behavior of high resistivity silicon detectors due to the presence of oxide charges," *Nucl. Instrum. Methods*, vol. A288, pp. 35–43, 1990.

[6] A. Castoldi and P. Rehak, "Electron drift time in silicon drift detectors: A technique for high precision measurement of electron drift mobility," *Rev. Sci. Instrum.*, vol. 66, pp. 4989–4995, 1995.